Postfrontal Airmass Modification

JEFFREY M. FREEDMAN AND DAVID R. FITZJARRALD

Atmospheric Sciences Research Center, University at Albany, State University of New York, Albany, New York

(Manuscript received 27 June 2000, in final form 23 December 2000)

ABSTRACT

The northeastern United States is subject to relatively frequent passages of frontal systems during the growing season. After a frontal passage, the newly arrived air mass is gradually modified by the underlying, mostly vegetated landscape. For the 1995–98 growing seasons, 25 frontal sequences with at least 4 days between frontal passages were identified; 16 had sufficient data continuity for rigorous analysis. A composite of sequences featuring the daily appearance of boundary layer cumulus clouds (BLcu) indicates a diminished role for entrainment and other external forcings because of the daily occurrence of a rapid growth phase in the mixed-layer (ML) diurnal evolution subsequent to day 1. Between frontal passages, net heat and moisture flux convergence in the ML is near zero, but during the warming and moistening phase, the surface flux terms, through a net radiation–BLcu feedback, are the principal controls on the tendencies of the ML temperature θ and specific humidity q. The combination of the θ and q tendencies leads to a nearly constant lifting condensation level, relative humidity, and BLcu cloud fraction during the latter part of the sequences. The presence of BLcu enhances water use efficiency and net afternoon carbon uptake throughout the sequence, with day 4 featuring optimal conditions. A multiday box model was used to perform sensitivity studies on subsidence, the lapse rate $\gamma_{\theta v}$ above the ML, cloud mass flux, and the regional surface Bowen ratio β_{reg}. The effects of subsidence and $\gamma_{\theta v}$ on ML processes are most conspicuous on day 1; during subsequent days, the rapid growth phase dominates the ML growth equation and reduces the impact of these external terms. Increasing β_{reg} to 3.5 reduces BLcu fraction to less than 20% and produces little net moistening of the ML, whereas reducing β_{reg} by 30% increases sequence BLcu coverage by 30%–80%. In sum, the presence of a net radiation–BLcu feedback allows for the establishment of an equilibrium in the ML heat and moisture tendencies and ensures the appearance of BLcu on each day of the sequence, thus sustaining favorable conditions for forest–atmosphere exchange (i.e., carbon uptake).

1. Introduction

During the spring–summer growing season, a procession of frontal systems moves across the northeastern U.S. region, ushering in drier and usually cooler air masses. The relatively frequent (usually one to two per week) passage of cold (or ''dry'') fronts has a cumulative impact on forest–atmosphere exchange, in that the periodic replacement of overlying air masses minimizes the potential for environmental stresses such as high surface temperatures and excessive vapor pressure deficits (VPDs). Forests locally modify these air masses through evapotranspiration (ET), injecting moisture into the atmosphere and facilitating the formation of boundary layer cumulus clouds (Freedman et al. 2001). Recent studies suggest that boundary layer cumulus clouds (BLcu), by modifying the light environment and tempering the buildup of heat, provide favorable conditions for carbon uptake (Freedman et al. 2001).

Sequences of undisturbed weather allow the mixed layer (ML) to accumulate heat, moisture, and atmospheric pollutants over a period of time, affecting local and regional surface–atmosphere exchange through feedbacks associated with environmental parameters such as VPD, insolation (through cloud shading), and air quality. The presence of a preexisting residual layer following the first day after a frontal passage allows for the rapid growth of the morning convective boundary layer and remixing of scalars from the previous day's diurnal cycle, facilitating the formation of BLcu. The existence of a nearly adiabatic residual layer beneath the capping inversion also diminishes the role of entrainment of air from the ''free'' atmosphere (FA) above in mixed layer growth and ML heat and moisture tendencies.

Airmass modification has been analyzed quantitatively by Burke (1945), and its theoretical underpinnings were set forth by Businger (1954). Both these studies focused on the case of cold air advection over warmer ocean waters, a frequent occurrence during the autumn and winter seasons off the east coast of the United States. Over land, airmass modification has usually been associated with the development of internal boundary

Corresponding author address: Jeffrey M. Freedman, Atmospheric Information Services, 251 Fuller Road, Albany, NY 12203.
E-mail: jmf@atmiserv.com

layers as air from one distinct region moves over a substantially different surface [e.g., lake → land; irrigated crops → nonirrigated grassland; see Oke (1987)]. Air pollution studies examine the modification of chemical constituents over several days, especially in the context of air stagnation (e.g., Su 1998; Zhang 1998). Here, the focus is on the transformation of an air mass through local (surface flux convergence into the boundary layer) and synoptic (advective) influences as it settles over the predominantly forested northeastern United States. Such sequences, to the authors' knowledge, have not been analyzed in the context of forest–atmosphere exchange—the cumulative effect of surface flux convergence and the modulation of the mixed-layer heat and moisture budgets by the presence or absence of BLcu.

Previous studies involving surface–atmosphere exchange characteristically examine a single diurnal cycle or a suite of unrelated days (Betts et al. 1996; Betts and Ball 1995) without considering the impact of airmass modification and accompanying thermodynamic feedbacks associated with accumulating heat and moisture in the ML. Thus, composites of ''golden'' days, chosen to accommodate remote sensing needs, are biased toward the ''best'' weather days, which usually occur after a frontal passage when a fresh air mass moves into a region (see Sellers et al. 1992, but cf. Sellers et al. 1995). During a typical growing season, more than 80% of ET and daytime net carbon uptake occurs on such days (Freedman et al. 2001). By analyzing a sequence of days, the effects of airmass modification and potential feedbacks within and above the mixed layer can be examined and a truer picture of mixed-layer dynamics over the course of several days is possible.

Here, a composited sequence featuring the daily appearance of BLcu is analyzed in terms of the ML heat and moisture budgets, including the surface sensible and latent heat fluxes (H and LE), carbon uptake, and transport terms, including advection, cloud mass flux, and subsidence. A multiday model sensitivity analysis is presented to examine the feedbacks among BLcu, the surface, ML, cloud layer, and the FA above.

2. Data

Since 1991, groups from the Atmospheric Sciences Research Center (ASRC) and Harvard University have made nearly continuous atmospheric turbulence and trace gas measurements at the Environmental Monitoring Site, a 30-m instrumented tower at Harvard Forest (HF), located in north-central Massachusetts (42.54°N, 72.18°W). The site topography features gently rolling terrain, varying between 300 and 350 m above sea level. The forest is 50–70 years old and contains a mixture of red oak, red maple, and hemlock. A variety of instruments record turbulent fluxes, solar and terrestrial radiation, temperature, humidity, wind profiles, and trace gas concentrations [see Sakai et al. (1997) and Moore et al. (1996) for further details]. An Automated Surface Observing System (ASOS) station operated by the Federal Aviation Administration is 10 km west-northwest of HF, at the Orange Municipal Airport (ORE). ORE is located in a bowl-shaped valley, open to the south, at an elevation of 155 m. The ASOS instrumentation (NWS 1998) is in a sandy area surrounded by grass and shrubs. Two runways and a taxiway are about 100 m away, with mixed woods surrounding the airport on three sides. The ORE ASOS data used in this study consist of hourly and special observations archived at the Department of Earth and Atmospheric Sciences of the University at Albany, State University of New York (UASUNY). Another ASOS station, located at the Worcester, Massachusetts, Regional Airport, is 39 km to the southeast of HF at an elevation of 308 m. These data consist of 5-min observations from the National Climatic Data Center. Sounding data are from upper-air observations made 2 times daily (2300 and 1100 UTC, or 1900 and 0700 LT) at Albany, New York (ALB), about 120 km to the west (the closest available upper-air station), and obtained from the National Climatic Data Center's Internet site (www.noaa.ncdc.com) or the National Weather Service Forecast Office in Albany (see Fig. 1). Surface and upper-air analyses were supplemented by the National Centers for Environmental Prediction (NCEP) Eta and Rapid Update Cycle model-initialized data, archived at UASUNY–National Center for Atmospheric Research and the NCEP reanalysis project (wesley.wwb.noaa.gov/reanalysis).

3. Methodology

a. Frontal case identification

Frontal cases were identified by examining time series of surface meteorological parameters and daily synoptic charts, using the traditional definition of a surface front (as depicted on daily weather maps): a transition zone between two air masses of different densities (Huschke 1959). A postfrontal sequence was defined as at least a 4-day period after the initial frontal passage and before the passage of the next significant synoptic system (usually another front). This minimum in sequence length was chosen to ensure synoptic influences could be separated from local contributions in the budget analysis. The first full day following a frontal passage was identified as ''day 1,'' with all cases having a frontal passage up to several hours before 2300 LT of the first day. Twenty-five cases were identified using this method. [This number, about six per season, is consistent with the anticyclone climatological statistics given in Harman (1987)]. Because of data problems (i.e., missing data from parts of a sequence for a dataset), 16 cases are used in this study, 5 each from 1995 and 1997 and 6 from 1998 (see Table 1). All cases had a sequence length of between 4 and 6 days. A composite length of 5 days was chosen, with day 6 of six cases averaged into day 5.

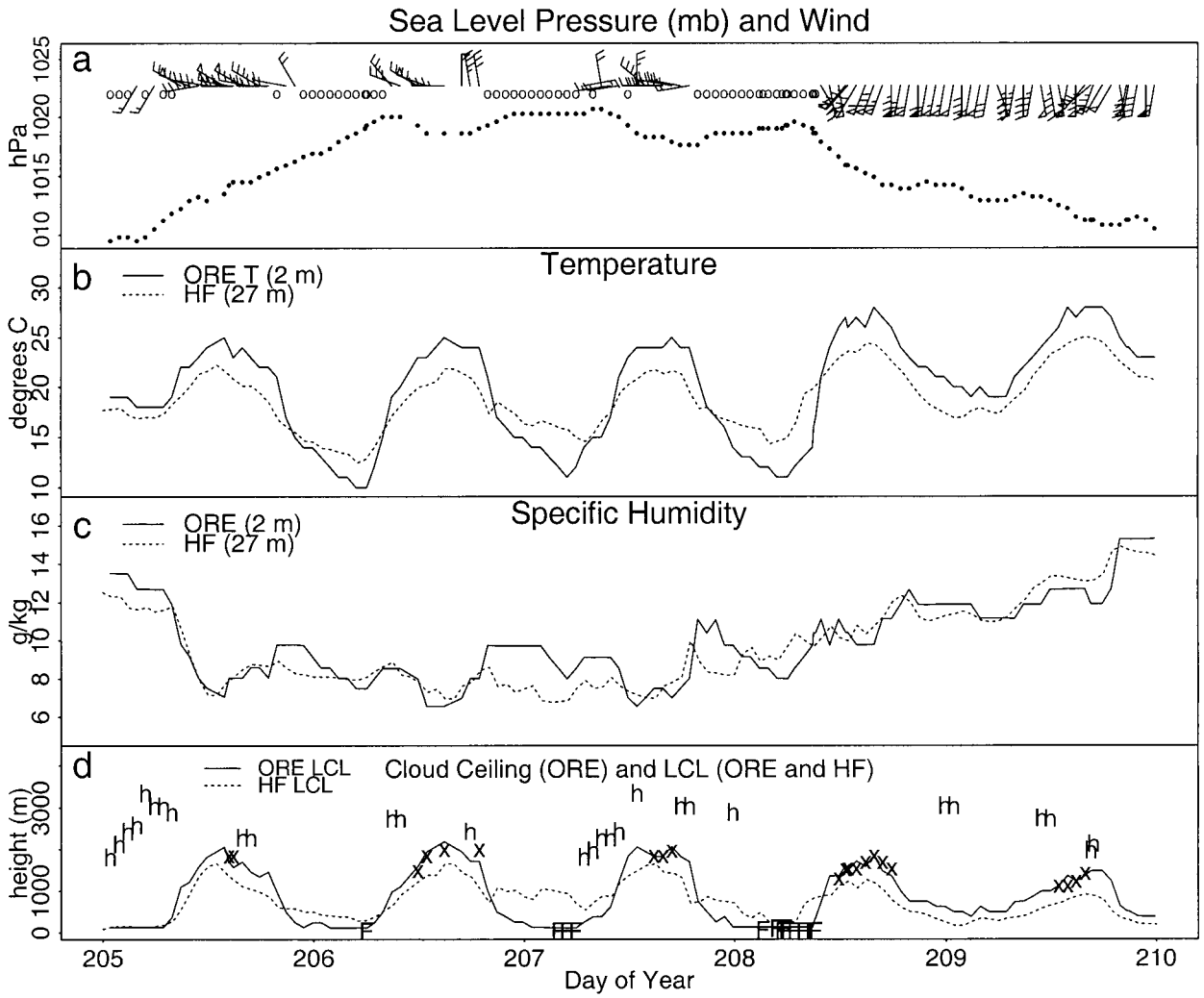

FIG. 1. Frontal sequence for days 205–209, 1998: (a) Orange, MA (ORE), sea level pressure (dotted line) and 10-m wind speed and direction (a single barb is 1 m s^{-1}), (b) ORE 2-m (solid line) and Harvard Forest (HF) 27-m (dotted line) temperature, (c) ORE 2-m (solid line) and HF 27-m (dotted line) specific humidity, and (d) ORE cloud ceiling (x: BLcu; h: high clouds; F: fog) and ORE (solid line) and HF (dotted line) LCL.

TABLE 1. Frontal cases, types, and source regions.

Date	Type	Source region of air mass
15–19 Jun 1995	Few clouds	Central Ontario
2–6 Jul 1995	BLcu	Great Plains
9–14 Jul 1995	BLcu	Midwest
30 Jul–2 Aug 1995	Few clouds	Southern Ontario
7–11 Aug 1995	Few clouds	Quebec
8–12 Jun 1997	Few clouds	Northern Great Plains
27 Jun–2 Jul 1997	BLcu	Midwest
10–15 Jul 1997	BLcu	Midwest
29 Jul–3 Aug 1997	BLcu	Saskatchewan–Manitoba
6–10 Aug 1997	BLcu	Midwest
2–5 Jul 1998	BLcu	Central Great Plains
11–16 Jul 1998	BLcu	Upper Midwest
24–28 Jul 1998	BLcu	Northern Great Plains
31 Jul–5 Aug 1998	BLcu	Saskatchewan–Manitoba
12–15 Aug 1998	BLcu	Ontario
19–23 Aug 1998	BLcu	Ontario

Source regions for air masses advecting into the Northeast were identified by back-trajectory analysis (going back 5 days from the beginning of the third day of a sequence) using the Hybrid Single-Particle Lagrangian Integrated Trajectory model, obtained at the National Oceanographic and Atmospheric Administration Internet site (www.arl.noaa.gov/ss/models/hysplit.html). They varied from the central and northern plains of the United States and Canada to Quebec (Table 1). These source regions are also consistent with the mean monthly anticyclone description of Harman (1987).

For a typical case, after frontal passage, drier and usually cooler air is advected into the region on northwesterly winds during day 1 (see Figs. 1a and 2a). Subsequent to passage, as a surface anticyclone moves into the northeastern United States, winds become light, and temperatures and humidity gradually increase (Figs. 1a,

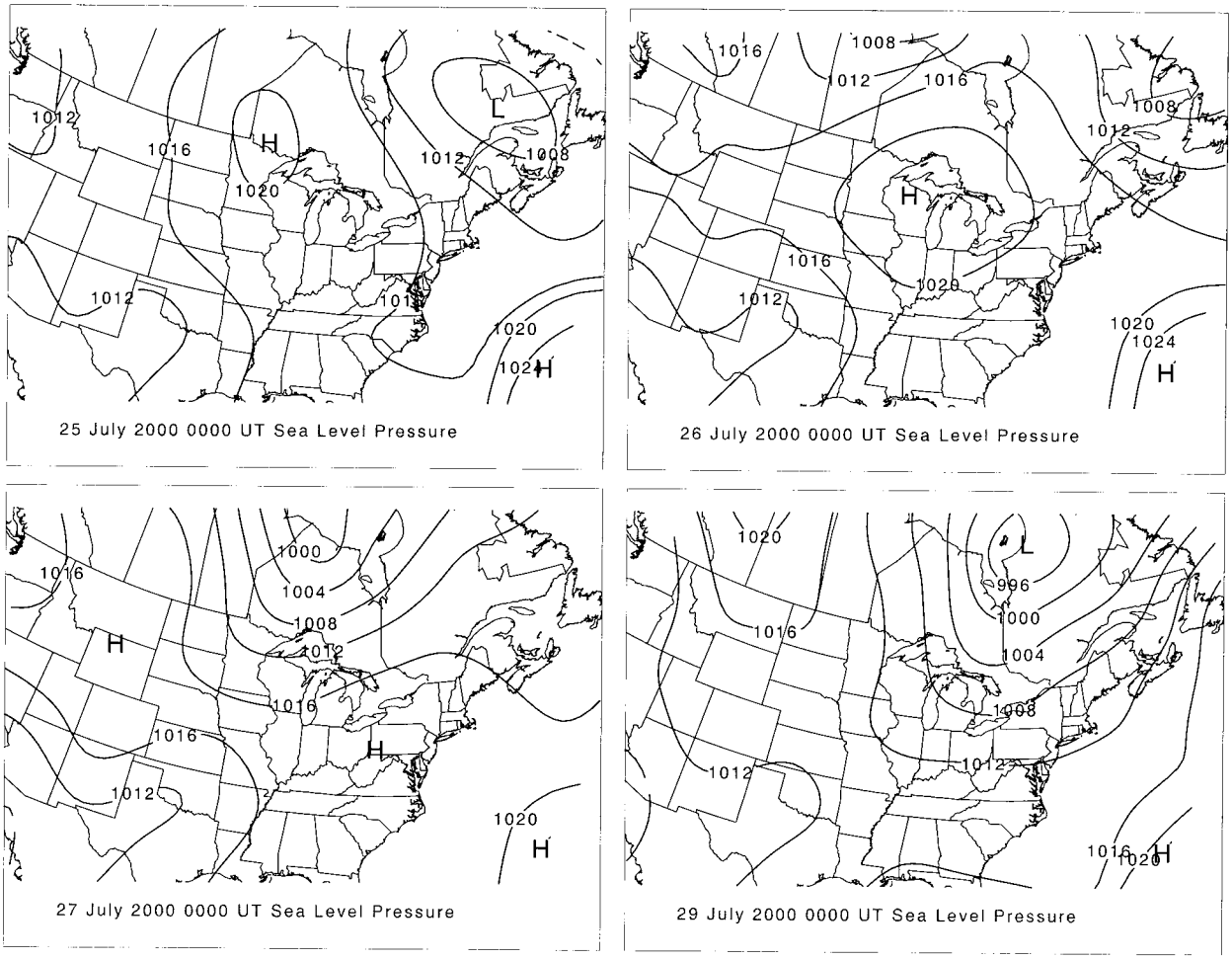

FIG. 2. Synoptic surface map with sea level pressure (hPa) for 24–28 Jul 1998 BLcu sequence.

2b, and 2c). As the high moves east, warmer and more humid air flows into the region on increasingly strong southwesterly winds ahead of the next frontal system (Figs. 1a, 1b, 2c, and 2d). Note that areas within several hundred kilometers southwest of HF and ORE are mostly forested.

From the remaining 16 cases, two case types were distinguished (see Table 1): those featuring the daily formation (at least two consecutive hours) of BLcu clouds (12 cases), as in Fig. 1 and those that were predominantly cloud free (''few clouds'') (4 cases).

b. HF–ORE site differences

Because many numerical weather prediction and climate models incorporate meteorological data from ASOS stations, the representativeness of these surface observations has implications for the efficacy of short-term forecasting of weather and air pollution events and longer-term climate prediction. For example, during typical afternoon convective conditions the surface-based lifting condensation level (LCL) is several hundred meters higher at ORE than that observed at HF (see Fig. 1d). Cloud ceilings, however, follow the ORE LCL, indicating that the most vigorous thermals (that tend to produce clouds) are generated over warmer, cleared areas (cf. MacPherson and Betts 1997). Both the LCL and BLcu cloud base are usually less than 20% above the height of the convective boundary layer (Stommel 1947; Stull and Eloranta 1985; Fitzjarrald and Moore 1994; Freedman et al. 2001); using the methods of Holtslag and van Ulden (1983, see section 5) to estimate the buoyancy flux and ML height z_i at ORE, the estimated ML height is much closer to the observed BLcu cloud base at ORE than at HF [details are given in the Freedman (2000) appendixes]. Given that the area surrounding and including HF and ORE is 85% forested (Foster 1992), ''hot spots'' such as developed lands (e.g., airports) are probably important sources of thermals able to reach their LCLs. Thus, one must be careful in choosing particular sites for making estimates of ML height, particularly in air pollution studies (e.g., Zhang 1998).

Differences in surface temperature between Harvard Forest and the Orange ASOS station (Fig. 1b) reflect dissimilar site characteristics and instrument heights. The ASOS temperature and humidity sensors at ORE

are 2 m above the surface. At HF, the top-level temperature and humidity measurements are 27 m above the surface and 5 m above the canopy top, or about 14 m above the displacement height. From surface similarity relationships for convective conditions (Paulson 1970; Deardorff 1972), the instrument height difference results in temperatures 0.5–1.0 K warmer at ORE, depending on sky and wind state. Given an assumption of an adiabatic lapse rate during convective conditions, the elevation difference between the two sites (about 150 m) accounts for an additional 1.5 K. The remaining daytime discrepancy, about 0.5–2 K, is probably related to the contrasting site attributes (i.e., the sensible heat flux at ORE is estimated to be 2 times that measured at HF; see discussion below). The specific humidity differences, however, are slight.

c. Mixed-layer budgets

The budget equations integrated across a mixed layer of thickness h are given by

$$\rho C_p \frac{\partial \overline{\theta}_m}{\partial t} = \frac{F_{\theta s} - F_{\theta i}}{h} + \rho C_p \left[-\mathbf{v} \cdot \nabla \theta_m - \overline{w}_h \left(\frac{\partial \theta_m}{\partial z} \right) - \left(\frac{\partial Q}{\partial z} \right) \right] \quad (1)$$

$$\rho L \frac{\partial \overline{q}_m}{\partial t} = \frac{F_{qs} - F_{qi}}{h} + \rho h L \left[-\mathbf{v} \cdot \nabla q_m - \overline{w}_h \left(\frac{\partial q_m}{\partial z} \right) \right], \quad (2)$$

where $F_\theta = \rho C_p \overline{w'\theta'}$ and $F_q = \rho L \overline{w'q'}$ are the heat and moisture fluxes, ρ is air density, C_p is specific heat capacity, θ is potential temperature, $\mathbf{v}$ is the horizontal wind, L is the latent heat of vaporization, m refers to mixed layer values, and s and i refer to the surface and mixed layer top. The first term in brackets is horizontal advection, $\overline{w}_h$ is the large-scale subsidence, $(\partial Q/\partial z)$ represents radiative flux divergence, and overbars denote mixed layer averages. After the approach of Garstang and Fitzjarrald (1999, p. 278), the large-scale subsidence in the mixed layer can be given as $\overline{w}_h = (1 - \sigma_c) w_{\text{env}} + \sigma_c w_{\text{ca}}$, where w_{env} is the environmental between-cloud subsidence, σ_c is the active cloud updraft area, and w_{ca} is the cloud updraft velocity.

Estimates of the radiative cooling rates were taken from Liou (1992, 393–396) using the equation

$$Q_{\text{s,ir}} = \eta Q|^{\text{ov}}_{\text{s,ir}} + (1 - \eta) Q|^{\text{clr}}_{\text{s,ir}}, \quad (3)$$

where Q is the net radiative cooling, η is the cloud fraction, the subscripts s and ir refer to solar and infrared heating or cooling rates, and the superscripts ov and clr refer to overcast and clear values.

During the first day of a frontal sequence, following a rapid cooloff and drydown, temperature and moisture advection diminish as the boundary layer grows into the new overlying air mass by entrainment (e.g., Garratt 1992; see Figs. 3 and 4a). During subsequent days, however, the diurnal boundary layer evolution proceeds in three phases. After sunset, a nocturnal boundary layer is established through creation of a surface inversion due to radiative cooling (SL in Fig. 3). Above this layer lies the residual mixed layer from the previous day (RL), and, if active clouds form, a cloud layer (CL) may be present, the thickness of which slowly decreases because of subsidence. Overnight, the net radiative flux divergence and subsidence terms usually balance (although the presence of clouds or residual moisture near the inversion overnight would favor cooling), leaving advection as the only potentially significant term (see Tables 2 and 3).

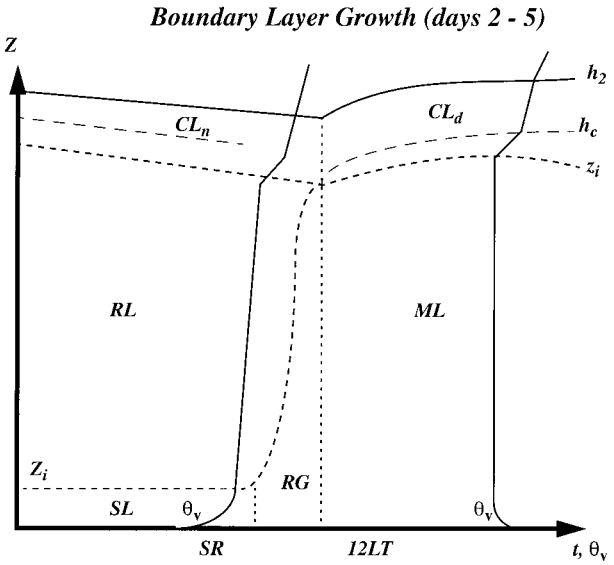

FIG. 3. Typical ML growth sequence during days 2–5 of frontal sequence. See text for details.

After sunrise, the nocturnal inversion breaks down, and the mixed layer grows rapidly into the previous day's residual layer (RG in Fig. 3). This growth takes place over a very short time, usually 1–2 h (see Deardorff 1974). During this growth phase, $\partial h/dt \approx 0.15 w_*$ (Deardorff 1974; Garratt 1992), where $w_* = (ghF_{\theta s}/\overline{\theta}_v)^{1/3}$, and this rapid energizing of the RL allows for the remixing of air from the previous day's fossil mixed-layer reservoir into the new ML.

During the afternoon phase dh/dt is negligible, and the entrainment fluxes are estimated by the relationships

$$F_{\theta_v i} = cF_{\theta_v s} \sim -\Delta\theta(-w_h) \quad \text{and} \quad (4)$$

$$F_{qi} = -\Delta q(-w_h), \quad (5)$$

as recognized by Ball (1960) and later by Tennekes (1973), Carson (1973), and Betts (1973). Here, $\Delta\theta$ and Δq represent the change in θ and q across the inversion, and c is a constant frequently given the value of 0.2 (e.g., Stull 1988, but cf. Betts and Barr 1996). Subsidence rates calculated from (4) and (5) above are generally within 20%–30% of those given by estimates from

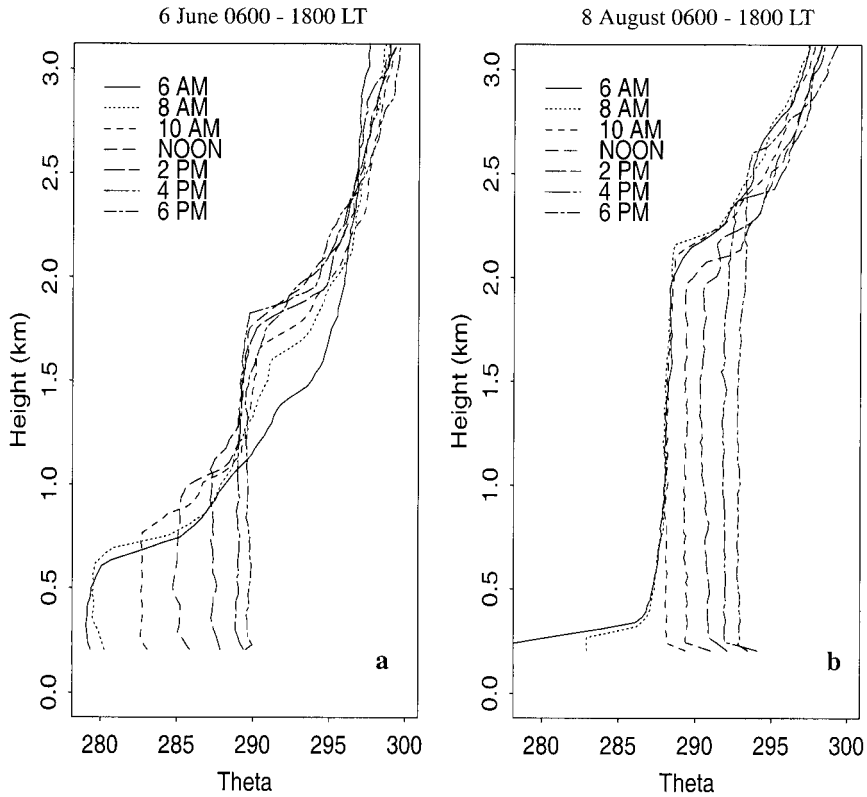

FIG. 4. BOREAS soundings from Thompson, MB, Canada, for (a) 6 Jun 1994, first day after a frontal passage, and (b) 8 Aug 1994, second day after a frontal passage.

the sounding sequence [from the technique of Carson and Stull (1986)], and the NCEP 850-hPa reanalysis (see Table 4).

At some point during the sequence, some clouds are able to reach the level of free convection (LFC). These clouds become ''active'' (Albrecht 1979; Stull 1985) and vent ML air into the lower FA, drying and warming the ML but cooling and moistening the cloud layer. Albrecht (1979) cites a maximum of 3% for the percentage of active cloud updrafts over the subtropical ocean. Here, the percentage of active clouds is assumed to be inversely proportional to the height of the LFC above the LCL, with a maximum of 3% (Albrecht 1979). A cloud updraft velocity w_{ca} of 1 m s^{-1} is also assumed.

TABLE 2. Mixed-layer heat budget for BLcu composite: day (0700–1900 LT) and night (1900–0700 LT) (K).

Day	$\partial\theta/\partial t$	$F_{\theta s}$	$F_{\theta i}$	$-\mathbf{v}\cdot\nabla\theta_m$	$w_h(\theta)$	$w_{ca}(\theta)$	$\partial Q/\partial z$
1 (day)	−1.70	1.72	0.33	−3.74	0.00	0.0	−0.08
(night)	−0.45	0.00	0.00	−1.77	2.15	—	−0.83
2 (day)	2.32	1.66	0.33	0.48	0.0	0.0	−0.15
(night)	−0.08	0.00	0.00	−0.44	0.97	—	−0.83
3 (day)	2.05	1.17	0.23	0.88	0.00	−0.1	−0.13
(night)	−0.43	0.00	0.00	−0.18	0.58	—	−0.83
4 (day)	2.69	1.70	0.34	0.94	0.00	−0.14	−0.15
(night)	−0.33	0.00	0.00	0.83	0.34	—	−0.83
5 (day)	2.72	1.70	0.34	1.36	0.00	−0.26	−0.42

The fractional cloud cover depends in part on the time required for inactive clouds to evaporate and mix with the environment (Albrecht 1981). For the purposes of this study, a steady state between active and decaying clouds is assumed.

Dividing (1) by (2) and implicitly including the terms in brackets gives a daily tendency Bowen ratio (Fitzjarrald et al. 2001) of

$$\beta' \equiv \frac{\rho C_p}{\rho L}\frac{h\dfrac{\partial\overline{\theta}}{\partial t}}{h\dfrac{\partial\overline{q}}{\partial t}}. \tag{6}$$

During sequences $\beta' \sim \beta \equiv F_\theta/F_q$, implying that the bracketed terms in (1) and (2) are either negligible or proportional to the surface flux (see below).

4. Observations

Results from a composite of frontal sequences that feature the near-daily appearance of BLcu follow.

a. BLcu cases

1) ML TRENDS

Although two distinct case types have been identified (sequences with BLcu and those with virtually no

TABLE 3. Mixed-layer moisture budget for BLcu composite: day (0700–1900 LT) and night (1900–0700 LT) (g kg^{-1}).

Day	$\partial q/\partial t$	F_{qs}	F_{qi}	$-\mathbf{v}\cdot\nabla q_m$	$w_h(q)$	$w_{ca}(q)$
1 (day)*	−5.35	1.15	−0.72	−4.92	0.00	0.00
(night)	0.01	0.00	0.00	0.47	−0.46	0.00
2 (day)	−0.01	1.10	−0.24	−0.86	0.00	0.00
(night)	0.71	0.00	0.00	0.95	−0.24	0.00
3 (day)	1.09	1.07	−0.21	0.23	0.00	−0.11
(night)	0.47	0.00	0.00	0.03	−0.28	0.00
4 (day)	1.48	1.28	−0.27	0.69	0.00	−0.22
(night)	0.08	0.00	0.00	0.23	−0.28	0.00
5 (day)	1.58	1.30	−0.23	1.08	0.00	−0.54

* For day 1, includes period from frontal passage on previous day through 0700 LT.

clouds), the number of few-clouds cases (four) precludes us from developing a composite. For the four years analyzed (1995–98), only one other such case was identified during the summer growing season (June–August), indicating the rarity of these events. However, analysis of the BLcu cases ($N = 12$) through the methodology of Brown and Hall (1999) (who use a modified t test to ascertain the robustness of means given a small sample) indicates that the means given in Tables 2 and 3 are significant at the 5% level (i.e., the composite means are not significantly different from the population parameters they are chosen from), thus taking a composite of these data seems reasonable. A qualitative comparison with the few-clouds cases is presented in Freedman (2000).

Several hours prior to 0000 LT of day 1 of the BLcu composite (the average time of frontal passage was 1630 LT the previous day, varying from 14 h prior to 3 h after 0000 LT of day 1) and into the afternoon of the first day, significant dry-air advection (~ -5 g kg^{-1}) occurs at the surface and aloft (Figs. 5c and 6b). This rapid drydown is typical of all the sequences analyzed. BLcu form readily as moderate winds ($\sim$3–6 m s^{-1}) out of the northwest combine with regional topography (see Freedman et al. 2001) and surface forcing to produce clouds (Fig. 5d). By the late afternoon of day 2, the surface pressure peaks, and the wind shifts into the southwest or south for the remainder of the sequence.

Throughout the sequence, superimposed on the diurnal cycle, the temperature moves steadily upward (Fig. 5b). For the humidity time series, the initial rapid drying during day 1 is followed by a gradual moistening of the overlying air mass. From day 2 onward, after sunrise but before the rapid growth phase, LE flux convergence produces a brief rise in the surface specific humidity (AJs in Fig. 5c). As the morning inversion dissipates, q falls rapidly during the late morning in response to vigorous remixing of drier residual-layer air downward, after which it remains constant or rises steadily during the afternoon. This q cycle has been observed by Martin et al. (1988), Mahrt (1991), and Betts (1992). During the early-evening transition, there is a jump in q (PJs in Fig. 5c) as residual positive LE flux (driven by plant transpiration) converges into the newly forming shallow nocturnal surface layer (Fitzjarrald and Lala 1989; Acevedo and Fitzjarrald 1999). Overnight, surface q falls, a likely result of dew deposition.

TABLE 4. Subsidence estimates (m s^{-1}).

Day	Soundings	NCEP	Budget	Used
1	−0.007	−0.011	−0.011	−0.010
2	−0.003	−0.005	−0.010	−0.0054
3	−0.006	−0.004	−0.007	−0.0047
4	−0.005	−0.002	−0.006	−0.0039
5	—	−0.002	−0.004	−0.0030

In response to both large-scale subsidence and increasing ML humidity, both z_i and the LCL fall from day 2 onward (Fig. 5d). BLcu onset time varies from 0900 to 1100 LT, within the rapid growth phase. There is a minimum in BLcu sky fraction on day 2, with a gradual increase during days 3 and 4 as both z_i and the LCL fall.

The heating and moistening of the mixed layer and the atmosphere above are evident in a composite time series of the 1100 and 2300 UTC (0700 and 1900 LT) soundings from ALB (Fig. 6). [Note that the evening soundings fail to capture the afternoon superadiabatic layer (Fig. 6a), and they also show some evidence of dew deposition (Fig. 6b).] Within the mixed layer, the heating and moistening rate is consistent with the surface values observed at ORE. Above the ML, changes in θ and q are about 1/3 and 1/2 of their ML values, or about the same as ML advection (Tables 2 and 3). From the θ and q profiles, there is a peak in ML height during day 2 ($\sim$2000 m) followed by a steady decline during the rest of the composite, a result of large-scale subsidence, an increasing cloud mass flux, and a decrease in the surface buoyancy flux after day 2.

Wyngaard and Brost (1984) showed that the ML scalar profile is related to the magnitude of the ratio of inversion level fluxes to the surface fluxes, given by $R = (w'c')_i/(w'c')_{s'}$, where c is either θ or q. For the moisture fluxes (not shown), R is initially greater than 0.5 but falls to about 0.3 by day 3. This may explain the differences in q profiles when comparing different field projects (see, e.g., Mahrt 1976, their Figs. 1 and 2; Garstang and Fitzjarrald 1999, their Figs. 5.14 and 5.16). Compositing only a select group of golden or ''clear'' days ignores the aggregate effects of airmass modification on the mixed layer and gives a biased picture of the thermodynamic structure of the boundary layer.

Recall the surface and inversion level fluxes from (1) and (2), $F_{\theta i} = \rho C_p(\overline{w'\theta'})_i$ and $F_{qi} = \rho L(\overline{w'q'})_i$. Both these terms involve the coupling of the θ and q gradients just below and through the inversion, where entrainment is taking place. Following the method of Betts (1992), we can estimate the inversion-level Bowen ratio through

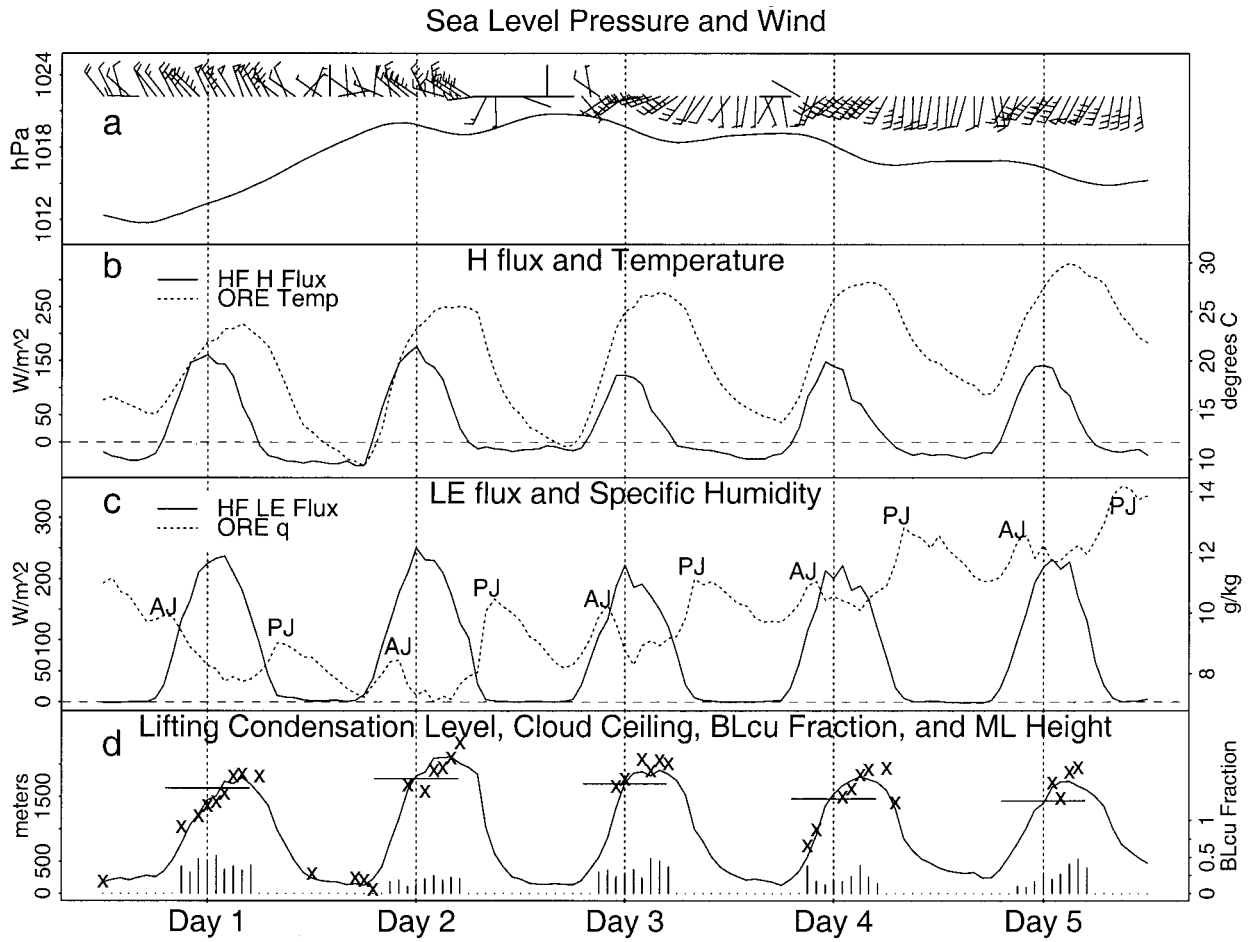

FIG. 5. Frontal composite for BLcu cases: (a) sea level pressure (hPa) and wind speed and direction (one barb equals 1 m s^{-1}), (b) HF H flux (W m^{-2}) and ORE 2-m temperature (°C), (c) HF LE flux (W m^{-2}) and ORE specific humidity [g kg^{-1}; AJ represents the morning jump and PJ is the evening jump in q (see text for explanation)], and (d) LCL and cloud ceiling at ORE [ML height is from ALB 2300 UTC (1900 LT) sounding].

$$\beta_i = F_{\theta i}/F_{qi} = (C_p/L)(\partial\theta/\partial q). \quad (7)$$

The results for the sequence, along with estimated (ORE) and measured (HF) surface fluxes, are given in Table 5. In general, entrainment drying (F_{qi}) is about 1/3 of the surface LE flux at HF, in good agreement with the profile analysis presented above.

2) ML BUDGET COMPONENTS

An important aspect of the tendency equations (1) and (2) is the contributions of each of the budget components to the overall trend in the surface-based LCL and ML RH and humidity. Ek and Mahrt (1994) derived an RH tendency equation to examine the relative contributions of diurnal boundary layer processes to the ML RH evolution. A modified form of this equation is given by

$$\begin{aligned}\frac{\partial(\mathrm{RH})}{\partial t} &= \alpha_1[(w'q')_s - c_q(w'q')_s] \\ &\quad - \alpha_1\left[\mathbf{v}_h\cdot\nabla q_m + w_h\left(\frac{\partial q_m}{\partial z}\right)\right] \\ &\quad + \alpha_2[(w'\theta')_s](1 + c_\theta) \\ &\quad - \alpha_3\left[\mathbf{v}_h\cdot\nabla\theta_m + w_h\left(\frac{\partial\theta_m}{\partial z}\right) + \frac{\partial Q}{\partial z}\right], \quad (8)\end{aligned}$$

where $c_\theta \equiv c = -(w'\theta')_i/(w'\theta')_s$, $c_q \equiv (w'q')_i/(w'q')_s$, $\alpha_1 = 1/hq_s$, $\alpha_2 = c_0\mathrm{RH}(dq_s/dT)(p/p_s)R/C_p$, $\alpha_3 = \mathrm{RH}(dq_s/dT)(p/p_s)R/C_p$, q_s is the saturation specific humidity, p is the pressure, and p_s is the surface pressure.

Equation (8) represents day-to-day changes of the afternoon minimum RH. Thus, the ML growth term included in Ek and Mahrt's Eq. (9) is negligible and is not included here. In general, net surface moisture flux convergence will tend to drive the RH higher (and the

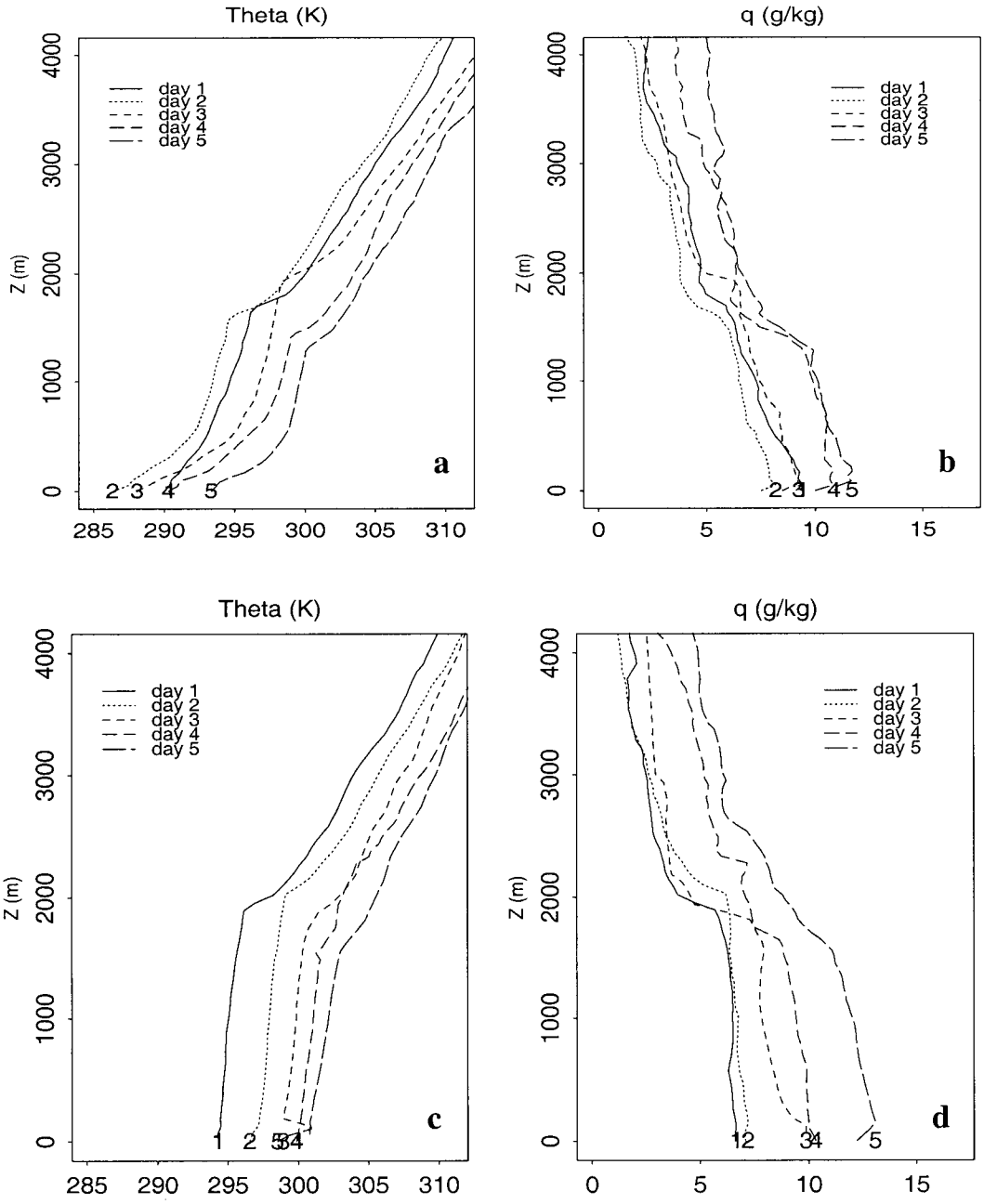

FIG. 6. Albany composite soundings for BLcu cases. (a), (b) 1100 UTC θ (K) and q (g kg^{-1}). (c), (d) As in (a) and (b) but for 2300 UTC.

TABLE 5. Estimated inversion strength, Bowen ratio, and surface and inversion fluxes (0700–1900 LT).

Day	$\Delta\theta$ (K)	Δq (g kg^{-1})	β_i (7)	β_i (budget)	$F_{\theta i}$ (W m^{-2})	F_{qi} (W m^{-2})	$F_{\theta s\ (\mathrm{ORE})}$ (W m^{-2})	$F_{qs\ (\mathrm{HF})}$ (W m^{-2})
1	2.06	−1.74	−0.47	−0.46	−33	70	163	175
2	2.02	−1.29	−0.64	−0.63	−34	54	172	171
3	1.57	−1.57	−0.41	−0.75	−28	37	139	147
4	1.11	−1.12	−0.41	−0.44	−31	70	154	158
5	1.43	−1.04	−0.57	−0.70	−31	54	154	176

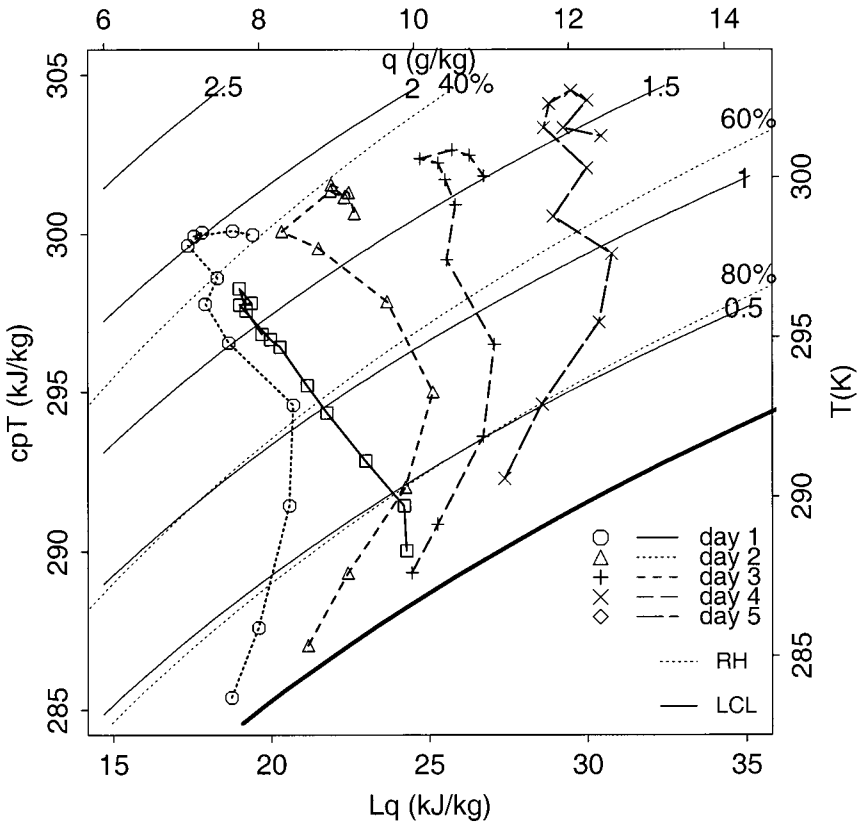

FIG. 7. Thermodynamic diagram of hourly daytime (0700–1800 LT) C_pT vs Lq (kJ kg^{-1}) or temperature (right axis; K) vs specific humidity (top axis; g kg^{-1}). Thin solid curves sloping upward represent a surface-based lifting condensation level (based on average surface pressure at ORE of 1000 hPa); thin dotted curves sloping upward to the right are relative humidity. Arrows in right corner are slope-based Bowen ratios.

LCL lower), whereas entrainment and subsidence will lower RH. Advection and cloud venting can either decrease or increase ML RH. Enhanced surface fluxes, a result of an increase in net radiation caused by the absence of clouds, would tend to drive RH lower and the LCL higher, because $\Delta(C_p\theta)$ effects are more significant than $\Delta(Lq)$ during the summer season. From Table 5, the moisture flux ratio throughout the BLcu sequence is always less than one (~0.25–0.45), which results in a positive contribution to the moisture tendency equation [(2)] from the $F_{qs,i}$ terms. A key question is how the other terms in (8) combine to determine whether clouds form.

Diurnal changes in θ and q can be illustrated on a conservative variable diagram, first introduced by Stommel (1947) and later used by Paluch (1979) and Betts (1984, 1985) to study entrainment into clouds and BL processes. For the BLcu composite (Fig. 7) with the exception of day 1 (when dry-air advection was dominant), there is an early to midafternoon *increase* in q (consistent with the above analysis of the inversion level fluxes) when the ML is convective and entrainment and any cloud mass flux represent a moisture sink. It may be that the afternoon drydown observed in previous work (e.g., Betts and Ball 1995) is an example of the first day following a frontal passage, when entrainment (and advection) drying effects are most vigorous, or is peculiar to sites particularly sensitive to rapid drying of soil moisture, such as prairie grasslands (Betts et al. 1999), or to canopy stress [i.e., the boreal forests; Moore et al. (2001)].

The magnitude and direction of the daily heat and moisture budget components are presented in vector form (Fig. 8). Here, the bracketed terms in (1) and (2) are bundled together into a ''transport'' term. Dry air advection initially dominates, but from day 2 onward, surface flux convergence is the principal control on the direction of the Ml θ and q tendencies. Furthermore, the overall tendency is toward a nearly constant RH and LCL. The ML moisture flux convergence accounts for 53% of the observed increase. For θ, the contribution from surface sources is 48%. If LE were reduced by 2/3, reflecting pre-leafout conditions, there would be little net gain in q for the entire sequence (see below). Because the majority of the growing season occurs during fair-weather recovery periods, this supports the results of Fitzjarrald et al. (2001), who found a nearly constant ''equilibrium''-tendency Bowen ratio [$\beta'_{eq} = 1/\varepsilon$RH,

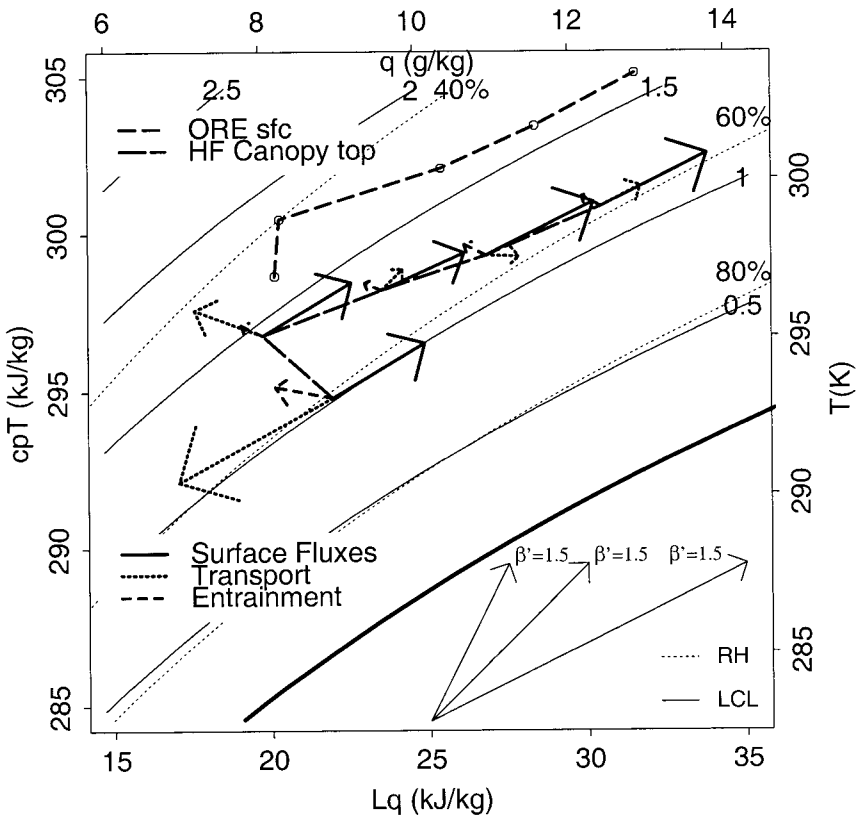

FIG. 8. Thermodynamic diagram for BLcu frontal composite. Thick solid line is for ORE; thick dotted line is for HF. Arrows represent contributions from surface fluxes (solid), transport terms (dotted), and entrainment (dashed).

where $\varepsilon = (L/C_p)(\partial q_{sat}/\partial T)$] during the summer growing season at Worcester. Budget analysis of (8) and model sensitivity studies (see below) show that the partition of the surface fluxes (Bowen ratio) and the areal coverage of active clouds determines what β' is maintained during a particular sequence.

b. Impact on forest–atmosphere exchange

Given the relative contributions of the surface flux and transport terms to the temperature and moisture tendencies, it is apparent that the net radiation–BLcu feedback plays a crucial role in the maintenance of nearly constant RH, LCL, and afternoon BLcu cloud fraction during the bulk of the sequence. Thus, an important question is whether the presence of BLcu is beneficial to forest–atmosphere exchange.

The cumulative impact of the divergent environmental conditions for the two case types is demonstrated in Fig. 9. Initially, net carbon (C) uptake was slightly higher on day 1 for the few-clouds sequences. Subsequently, the more extreme conditions exhibited during the few-clouds cases (in terms of VPD and surface temperatures) result in progressively smaller net C uptake until day 5, when conditions abate somewhat as the VPD, in response to strong surface moisture advection, decreases. Conversely, during the BLcu sequence, the presence of clouds and the static environmental conditions allow for a steady increase in afternoon net C uptake, with a *maximum* on day 4. As ET was about 20% greater during the few-clouds composite (there was no evidence of water stress, probably because of the buffering effect of deep soil moisture), water use efficiency (WUE), defined here in terms of the carbon dioxide (CO_2)–water vapor flux ratio F_{CO2}/ET (Rosenberg 1983), was much higher during the BLcu composite, especially during days 2–4. On day 4, net uptake is 50% higher, WUE is doubled, and the VPD is 8 hPa less for the BLcu sequence. The key result of the above observations is the *opposing trends* in afternoon uptake and WUE. The effect of persistently higher VPDs and surface temperatures is a reduction in net afternoon C uptake and a decrease in WUE. In contrast, the daily presence of clouds retards the heating of the ML, thereby reducing the VPD, and allows for the deeper penetration of light into the forest canopy, increasing WUE.

Baldocchi (1997) observed that the lack of clouds allows leaves at the top of the canopy to become warmer and more light saturated than leaves in the lower canopy. Consequently, these leaves experience enhanced respiration, which lowers rates of net photosynthesis (Baldocchi and Harley 1995). Moreover, high VPDs lead to

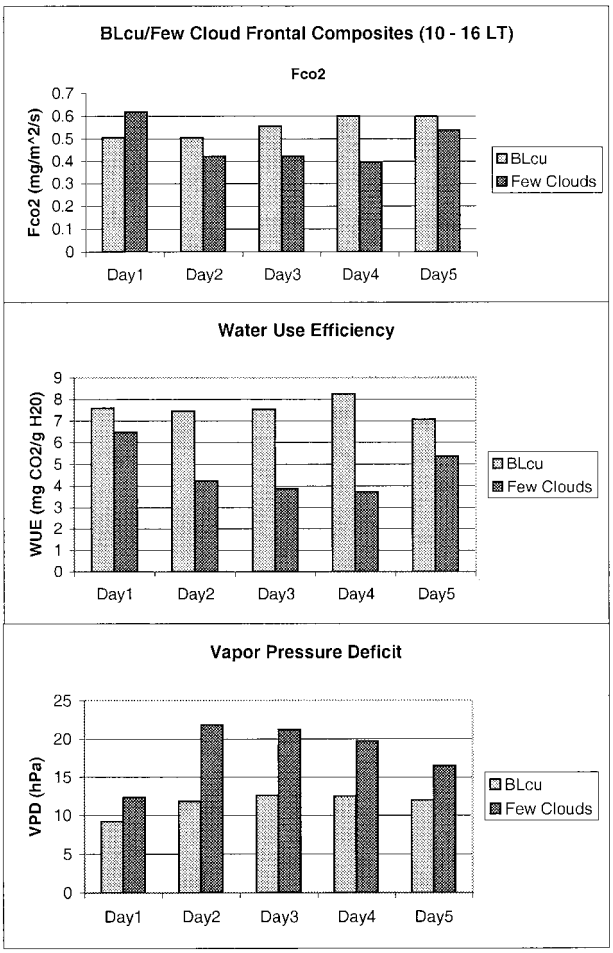

FIG. 9. (a) Comparison of midday (1000–1600 LT) F_{CO2} (mg m^{-2} s^{-1}) for BLcu and few-clouds sequences; (b) as in (a), but for WUE [mg CO_2 (g H_2O)$^{-1}$]; (c) as in (a), but for VPD (hPa).

stomatal closure, further limiting C uptake (Rosenberg et al. 1983). Cardon et al. (1994) and Barradas and Jones (1996) have shown that some plants have higher WUEs in fluctuating light environments, a consequence of favorable states of stomatal closure and carbon fixation.

The accumulated stress of high temperatures, high VPDs, and light saturation undoubtedly contributed to the steady reduction in afternoon F_{CO2} through day 4 of the few-clouds sequence. That such a relatively short sequence of cloudless days featuring increasingly hot, dry conditions can significantly reduce net C uptake and WUE means any prolonged drought would likely have a deleterious impact on forest–atmosphere exchange.

5. Modeling study

The purpose of performing the following model sensitivity study is to examine the role of surface and external forcings in modifying θ and q and hence RH and the LCL. Because only standard meteorological data are available at ORE, an estimate of the buoyancy flux is needed to predict the height of the ML. The methodology of Holtslag and van Ulden (1983) and De Bruin and Holtslag (1982) is used to estimate H. A simple jump model (Driedonks 1982; Garratt 1992) is then used to estimate the ML height, and it includes predictive equations for θ and q. The ML growth equations include subsidence, horizontal advection, and cloud mass flux terms and incorporate a rapid morning ML growth parameterization for days 2–5 (Deardorff 1974; Garratt 1992). Surface similarity relationships are then used to estimate surface temperature and humidity (see section 3b). A radiation feedback relating BLcu cloud cover to the fraction z_i/LCL (Freedman 2000) is used as a control on the magnitude of the surface fluxes. Last, the active cloud fraction is assumed to vary inversely with the depth of the layer between cloud base and the level of free convection (LFC − LCL), with a maximum of 0.03 (Albrecht 1979).

TABLE 6. Model input (control).

Day	q_{FA} (g kg^{-1})	$\gamma_{\theta v}$ (K m^{-1})	w_h (m s^{-1})	σ_c
1	4.23	0.005 47	−0.010	0.0
2	4.37	0.006 01	−0.0054	0.0
3	5.79	0.005 09	−0.0047	0.005
4	6.64	0.006 22	−0.0039	0.015
5	7.74	0.005 58	−0.0015	0.03

a. Control case

Initial conditions for external parameters are taken from the BLcu composite analysis and used as input to the model for the control case and are given in Table 6. The daytime trend and magnitude of cloud fraction compare reasonably well with the observations, although model sky cover is slightly higher (1/10–2/10) during midday (not shown). This is likely due to the weakness of the parameterization relationship during the rapid growth phase, when z_i is growing more quickly than the surface-based LCL. Also, valley-induced circulations may result in a minimum in sky fraction at ORE, which would occur during the time of strongest buoyancy fluxes.

For the q sequence, the differences between the control case and observations at HF and ORE are less than 0.5 g kg^{-1} (Fig. 10). The morning rise and midday fall in q seen in the observations (notable at ORE) are captured by the model, although the afternoon decrease is overestimated ($\sim$0.5 g kg^{-1}) on days 4 and 5. The evening q jump compares well with HF but is underestimated at ORE.

The heat and moisture tendencies observed in Fig. 8 are simulated well by the model-generated fluxes (see Figs. 11–13). There is a slight warm bias in the model, which, combined with the underestimates of q on days 4 and 5, produces afternoon maximum LCLs that are about 100–200 m higher than are observed at ORE.

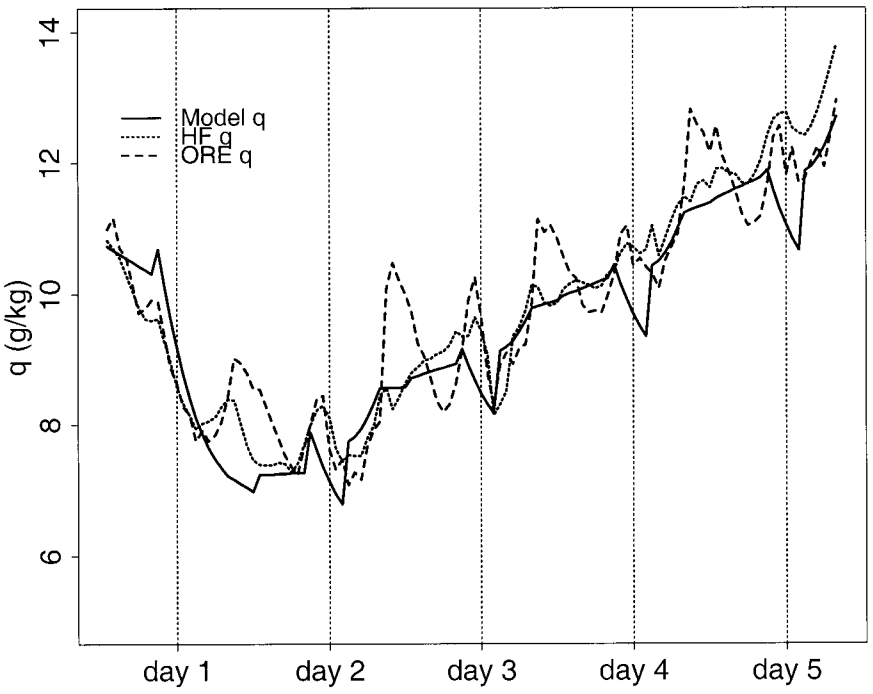

FIG. 10. Model (solid line), HF (dotted), and ORE (dashed) specific humidity (g kg^{-1}) for control case.

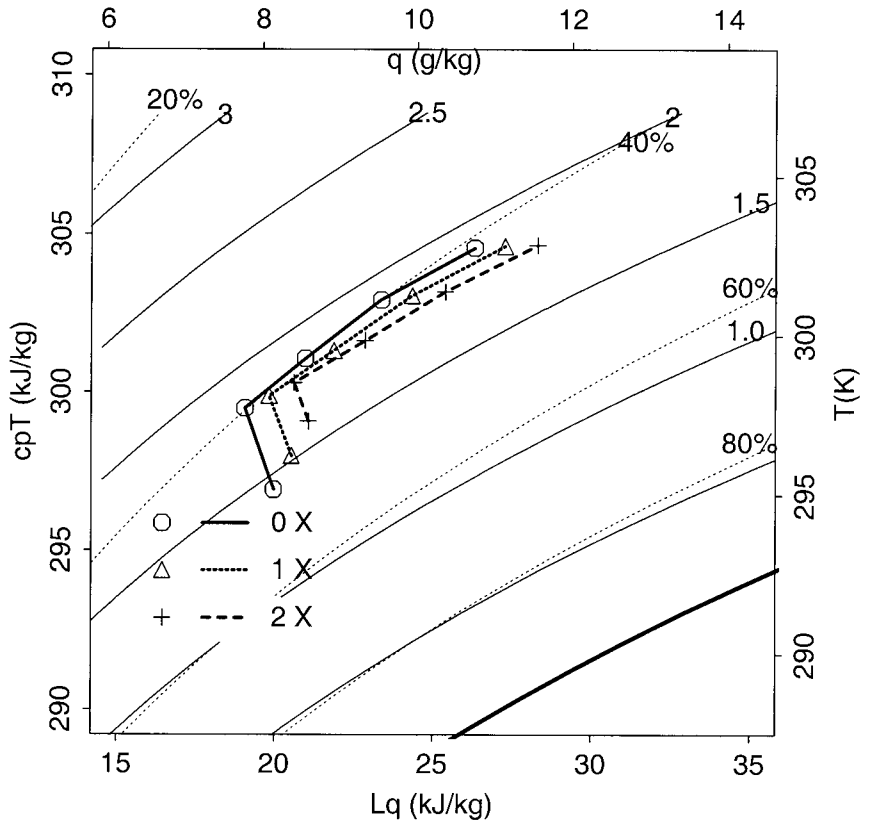

FIG. 11. Thermodynamic diagram (C_pT, Lq) for no-subsidence case (circles and solid line), control case (triangles and dotted line), and doubled-subsidence case (pluses and dashed line).

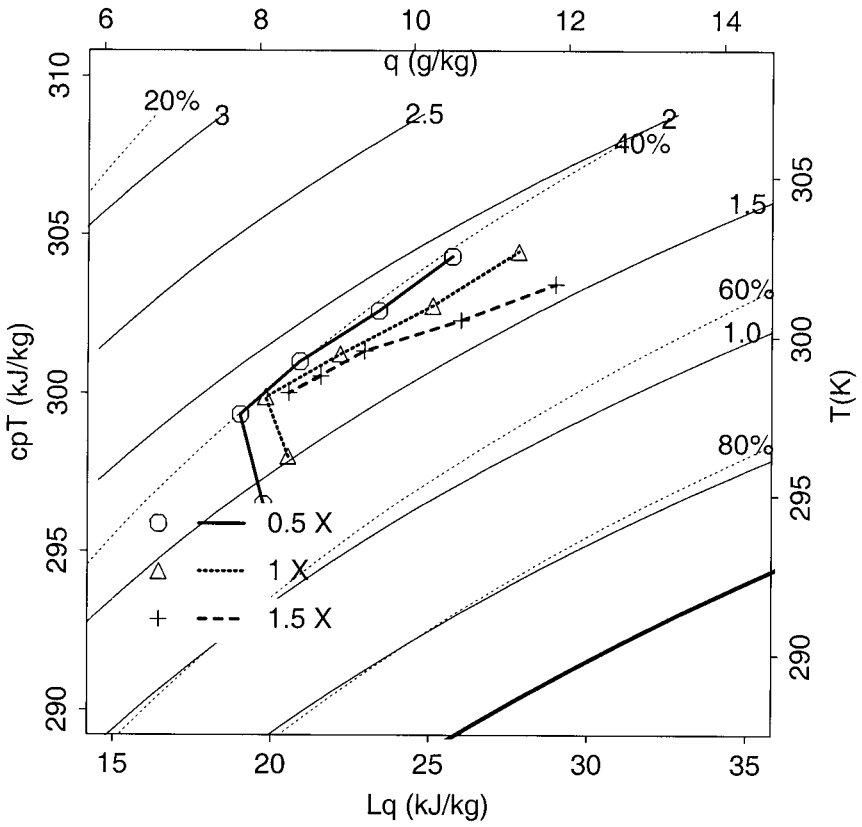

FIG. 12. Thermodynamic diagram for 50% FA lapse rate and enhanced active cloud area case (circles and solid lines), control case (triangles and dotted lines), and 150% control FA lapse rate and no active clouds case (pluses and dashed lines).

b. Subsidence

According to (8), changes in large-scale subsidence can either increase or decrease ML RH, depending on the magnitude and location of the $C_p\Delta\theta$ and $L\Delta q$ terms on the thermodynamic diagram. Temperature and humidity tendencies for all three model runs combine to produce an almost constant RH, LCL, and β' from day 2 onward (Fig. 11). Furthermore, the results show decreasing variation in z_i for either the doubling or no-subsidence case (Table 7), in response to the decreasing rates of subsidence and smaller variability in sky cover. Day 1 has the greatest variability in sky cover, with the no-subsidence case allowing for higher z_i and lower LCL than the control case (~250 m). For days 2–4, small changes in sky cover [0.1 higher (lower) for the no (doubled)-subsidence case] with increased subsidence are evident, a response to the competing effects of warming (cooling) and drying (moistening) associated with deeper (shallower) MLs. However, by day 5 this pattern reverses, a result of the increased influence of active clouds venting moisture out of the ML, thereby increasing the LCL.

c. The $\gamma_{\theta v}$ (free-atmosphere lapse rate) and cloud mass flux

Most boundary layer growth models are very sensitive to changes in $\gamma_{\theta v}$, because the term appears in the denominator of most growth equations and its magnitude is very small (on the order of 0.005 K m^{-1}). Time variations in $\gamma_{\theta v}$ occur primarily through changes in large-scale subsidence, radiative flux divergence, and advection.

Unlike over the subtropical oceans, the cloud layer associated with daytime active cumulus clouds over land is likely transitory in nature. For the BLcu composite, $\gamma_{\theta v}$ never varies by more than 5% from day to day, and cloud layer heating and moistening never exceed 0.3 K and 0.5 g kg^{-1}. During the few-clouds sequences, $\gamma_{\theta v}$ was consistently 30% greater than what was observed during the BLcu cases; thus, initial conditions, such as the magnitude of large-scale divergence associated with a particular air mass, likely determine the evolution of $\gamma_{\theta v}$ during a frontal sequence.

Because the ability of cloud updrafts to reach their LFCs is partially dependent upon $\gamma_{\theta v}$, the magnitude of the active cloud fraction term is linked with the $\gamma_{\theta v}$ sensitivity. Thus, for the enhanced $\gamma_{\theta v}$ case, the active

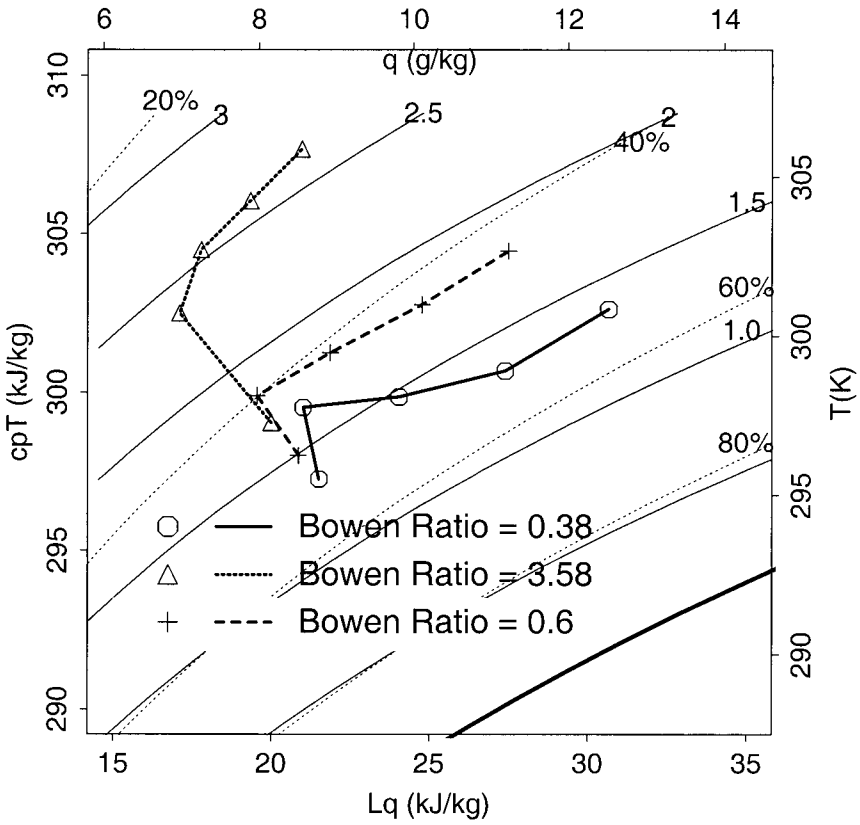

FIG. 13. Thermodynamic diagram for regional Bowen ratio sensitivity: solid line (β_{reg} = 0.38), dashed line (β_{reg} = 0.6), and dotted line (β_{reg} = 3.58).

cloud fraction is set to zero throughout the sequence. Alternatively, for the reduced $\gamma_{\theta v}$ case, active clouds appear during all 5 days of the sequence, with the updraft area doubling during days 3–5.

With a 50% increase in $\gamma_{\theta v}$ (Table 7), day-1 BLcu cloud cover remains below 20%. Suppressed ML heights result in an increase in surface temperatures, but dry-air advection reduces the effect of ML q convergence, resulting in an LCL nearly 500 m higher (Fig. 12). Subsequently, z_i varies less with time from the control case, a function of the rapid-growth parameterization and the absence of cloud venting (by day 5, z_i is actually a few meters higher than in the control case). This results in progressively higher q for the remainder of the sequence and higher values of BLcu sky fraction with time. By day 5, BLcu cloud fraction is 50% *greater* than the control case.

Fitzjarrald (1982, 1997), using a variation of a simple airmass modification model originally developed by Businger (1954, chapter 3), showed that strong stability aloft depresses ML growth and accelerates the saturation of the ML by limiting its depth and entrainment of warm air from the FA. Here, once the countereffects of dry-air advection cease (and with the absence of a cloud mass flux), similar results are seen, with decreased ML heating because of the increase in cloud cover, which contributes to a lowering of the LCL.

For a 50% reduction in $\gamma_{\theta v}$, consistently higher ML

TABLE 7. Model results [afternoon z_i (m) and cloud cover].

		Day 1		Day 2		Day 3		Day 4		Day 5	
Case	Sensitivity	z_i	BLcu	z_i	BLcu	z_i	BLcu	z_i	BLcu	z_i	BLcu
Observed		1660	0.45	1870	0.27	1770	0.37	1590	0.31	1510	0.41
Control		1522	0.41	1713	0.37	1697	0.42	1598	0.39	1564	0.38
Subsidence	(0)	1658	0.59	1846	0.44	1842	0.47	1735	0.38	1675	0.37
	(2 x)	1392	0.28	1583	0.31	1576	0.35	1534	0.33	1510	0.35
γ-mass flux	(0.5 x)	1711	0.49	1916	0.52	1912	0.54	1796	0.46	1768	0.44
	(1.5 x)	1286	0.18	1594	0.33	1597	0.39	1576	0.47	1608	0.59
Bowen ratio	3.58	1496	0.33	1804	0.23	1863	0.22	1809	0.19	1834	0.19
	0.38	1257	0.35	1513	0.5	1465	0.67	1321	0.56	1263	0.52

heights are produced throughout the sequence. BLcu cloud cover is much higher during days 1–3, a response to cooler ML temperatures (and lower LCLs) as dry-air advection reduces the impact of diminished moisture flux convergence. By days 4 and 5, however, an enhanced cloud mass flux combined with deeper MLs raises the LCL 200 m above the control case, but afternoon ML growth and moisture flux convergence result in higher cloud cover than in the control case.

d. Regional Bowen ratio (β_{reg})

Different atmospheric and surface conditions (drought, excessive precipitation) may result in varying fluxes at both HF and ORE. Over the forested regions surrounding ORE and HF, extended periods of drought can reduce ET by more than 30% (e.g., Freedman et al. 2001). Furthermore, land use patterns have changed considerably in the preceding years around HF [forest cover has increased from 25% to 85% since the 1830s; Foster (1992)], and changes in land cover type will affect the regional energy partition. Just before the start of the growing season, the highest midday Bowen ratios ($\sim$3), sensible heat fluxes ($\sim$250 W m^{-2}), and mixed-layer heights ($\sim$1400 m) occur at HF and ALB (Moore et al. 1996; Sakai et al. 1997; Freedman et al. 2001). Frontal sequences during this time feature little net moistening and few BLcu. During the growing season, however, β is about 0.6, H is about 100 W m^{-2}, and z_i is about 1200 m. By varying H_{ORE} and $\mathrm{LE}_{\mathrm{HF}}$, the regional Bowen ratio (i.e., $\beta_{\mathrm{reg}} = \mu_1 H_{\mathrm{ORE}}/\mu_2 \mathrm{LE}_{\mathrm{HF}} + \mu_2 H_{\mathrm{ORE}}/\mu_1 \mathrm{LE}_{\mathrm{ORE}}$, where $\mu_1 = 0.1$ and $\mu_2 = 0.85$ represent land use fractions for cleared and forested areas) can be perturbed to assess the net radiation–BLcu feedback and consequent changes in the θ and q tendencies.

Higher β_{reg} produces increased ML heights and minimal sky cover (Table 7). Warmer temperatures and no net moistening in the ML (Fig. 13) produce much higher LCLs (nearly 1 km higher by the end of the sequence as compared with the control case). The combination of a higher z_i and much higher LCL results in a virtual absence of clouds (and hence a much reduced cloud mass flux) throughout the sequence. Despite nearly clear skies and high values of net radiation, low values of LE result in a decrease in ML RH. Thus, the lack of clouds and transpiring vegetation eliminates a mechanism whereby heat and moisture flux convergence combine to maintain a nearly constant LCL.

Decreasing the regional Bowen ratio to 0.3 (or increasing the $\mathrm{LE}_{\mathrm{HF}}$ flux by 10%–30%) results in a 50% increase in BLcu sky fraction for days 2–5 of the sequence. The reduced heat flux, increased moisture, and cloud mass flux produce lower MLs (up to 250 m), lower temperatures, and higher q, giving LCLs about 500 m lower than in the the control case by day 5. Between days 2 and 4, there is a significant decrease in the LCL (400 m) and corresponding increase in ML RH, as moisture flux convergence dominates and temperatures rise very little in response to the reduced sensible heat flux.

e. Surface–ML equilibrium

Eliminating the large-scale transport terms (advection and cloud mass flux) and extending the model run out to 8 days indicates that the surface–ML equilibrium is reached by day 3 of the sequence, after the establishment of the residual layer and diminishment of entrainment effects. Furthermore, exclusion of clouds in the model shows that this surface—ML equilibrium is still maintained; β does not change, but the magnitude of the fluxes increases (this was observed during the few-clouds sequences); however, if a vegetation stress feedback is included [by the canopy resistance relationship in the Penman–Monteith formulation (Monteith and Unsworth 1990)], an equilibrium is still achieved but at a significantly higher LCL ($\beta' \sim 1.3$) as the $C_p \Delta\theta$ term becomes dominant. The key point, therefore, is that the presence of a net radiation–BLcu feedback allows for the establishment of a smaller β' and thus ensures the appearance of BLcu on each day of the sequence, thus sustaining favorable conditions for forest–atmosphere exchange (i.e., carbon uptake).

6. Summary and conclusions

Fair-weather days that constitute the bulk of the time during frontal sequences account for more than 80% of ET and net C uptake during the growing season. Modification of the heat and moisture characteristics of air masses during sequences is crucial to tempering potential stresses to vegetation such as surface temperature and VPD. The net radiation–BLcu feedback mechanism is the key control in modulating the buildup of heat and moisture during sequences.

The heterogeneity of the land surface in the northeastern United States, with small areas of cleared lands intermixed with larger areas of forest tracts, facilitates the formation of BLcu as more energetic thermals that develop over cleared, warmer surfaces are amply supplied with moisture from the surrounding forested regions. Thus, at least in the northeastern United States, BLcu onset and coverage is not based on a simple choice of cleared versus forested lands dependent upon initial thermodynamic ML profiles (e.g., Rabin et al. 1990); rather, sufficient source regions of energetic thermals combined with topography (see Freedman et al. 2001) and freely transpiring vegetation acting in concert with the net radiation–BLcu mechanism ensure that on most days during a frontal sequence cumulus clouds will appear. The occurrence of consecutive clear days during the growing season is a rare event, confined to periods of extreme drought, an influx of unusually dry air masses, and reduced ET (see Freedman 2000).

Because most observational and modeling studies focusing on surface–atmosphere exchange examine indi-

vidual diurnal events or a suite of unrelated days, the role of entrainment and its effect on surface–atmosphere exchange (i.e., the saturation deficit) is often exaggerated (see e.g., Raupach 1991; Raupach and Finnigan 1988; McNaughton and Spriggs 1985). This is due to the assumption that the ML is always growing by entrainment, thus ignoring the remixing of scalars during the rapid-growth phase of ML height evolution. Every day is treated as day 1 of a sequence. Furthermore, most large-scale field projects that examined the linkage between surface processes and ML dynamics have occurred in areas that feature significant constraints on ET [such as the First International Satellite Land Surface Climatology Project Field Experiment (FIFE) and the Boreal Ecosystem–Atmosphere Study (BOREAS)]: deeper MLs and limited moisture result in afternoon drydowns during fair-weather days or during a sequence of days (Betts et al. 1999). In the eastern United States, however, where forested areas supply ample moisture to the ML, surface moisture flux convergence accounts for 50% of the gross gain in the ML moisture budget during a typical sequence. Entrainment drying accounts for less than 20% of the total ML moisture tendency, in stark contrast to findings of other field studies (e.g., FIFE and BOREAS).

The finding that the heat and moisture budget components combine to achieve a nearly constant LCL, RH, and BLcu cloud fraction during the sequences indicates that the net radiation–BLcu cloud cover feedback operates to sustain an equilibrium β' that maintains fairly constant afternoon BLcu cloud fraction. This feedback regulates ML growth and thermodynamic tendencies, tempers the buildup of ML temperatures (and hence the VPD), and, through the daily appearance of BLcu, provides a daily dosage of enhanced diffuse radiation to the forest interior, producing a more favorable environment for C uptake.

The BLcu enhancement is not included in most global primary production models, which estimate rates of C uptake as a product of radiation use efficiency and a satellite-derived estimate of solar radiation absorbed by canopies (see Baldocchi 1997; Ruimy et al. 1994). Because the effects of BLcu cloud cover are not included in these models, net ecosystem exchange can be over- or underestimated, depending upon local sky conditions.

The model sensitivity analysis presented above highlights the importance of including a rapid growth parameterization in multiday ML growth models. The modeling study has shown, however, at least for the summer growing season, that compensating effects of heating and moistening or cooling and drying produce little change in sky cover and hence in the surface fluxes that control the LCL and RH tendencies. A similar result was found when varying the temperature stratification above the ML. Although large day-to-day variations in $\gamma_{\theta v}$ are rare in the real atmosphere, it is noteworthy that significant differences in external forcings produce compensatory changes in ML θ and q; surface fluxes are thus insensitive to such perturbations because of the z_i/LCL relationship.

In contrast, changes in the regional surface Bowen ratio are directly linked to the net radiation–BLcu feedback, and hence ML dynamics are very sensitive to altering β_{reg}. On a seasonal level, an increase in BLcu frequency occurs after the decrease in β at HF (Freedman et al. 2001; Sakai et al. 1997; Moore et al. 1996) associated with the commencement of transpiration. The relevance of this observation to the airmass modification question is borne out in the modeling analysis using preleafout β values that show a reduction in BLcu cloud cover to below 20% for the entire sequence. A slight decrease (from 0.6 to 0.4) in β_{reg} from typical growing season values produces an acceleration in ML moistening and much higher BLcu cloud cover (50%–75%). Thus, changes in the *partitioning* of the surface fluxes can lead to large perturbations in the mixed-layer thermodynamic state and the probability of BLcu formation. This fact has important implications for modeling studies that consider the effects of land use changes on surface–atmosphere processes (see, e.g., Pielke 2000).

Northeastern forests are acclimated to frequent passage of cold or dry fronts during the growing season. These passages provide a regular series of cooler and drier air masses to the region; local and regional airmass modification then allows for the formation of BLcu. Any change in local land use patterns (or changes in the airmass source regions) that produces a decrease in the frequency of BLcu (which tend to mitigate extreme conditions and enhance net carbon uptake) may adversely affect the health of the forest ecosystem and permanently alter the regional climate.

Acknowledgments. Primary support for this work is from the Joint Program on Terrestrial Ecology and Global Change of the National Aeronautics and Space Administration (NAG 56227) to the Research Foundation of the State University of New York. Flux observations by ASRC at Harvard Forest are supported by the U.S. Department of Energy's (DOE) National Institute for Global Environmental Change (NIGEC) through the NIGEC Northeast Regional Center at Harvard Forest (DOE Cooperative Agreement DE-FC03-90ER61010), under Subcontract 901214 from Harvard University. We are grateful to J. W. Munger and S. C. Wofsy of Harvard University for sharing data and other resources with us. We appreciate the efforts of personnel at the Albany National Weather Service Forecast Office in providing us with some of the Albany sounding data. We acknowledge the assistance of John Sicker, who provided excellent technical support throughout the term of this study.

REFERENCES

Acevedo, O. C., and D. R. Fitzjarrald, 1999: Observational and numerical study of turbulence during early evening transition. Pre-

prints, *13th Symp. on Boundary Layers and Turbulence,* Dallas, TX, Amer. Meteor. Soc., 96–99.
Albrecht, B. A., 1979: A model of the thermodynamic structure of the trade-wind boundary layer: Part II. Applications. *J. Atmos. Sci.,* **36,** 90–98.
——, 1981: Parameterization of trade-cumulus cloud amounts. *J. Atmos. Sci.,* **38,** 97–105.
Baldocchi, D., 1997: Measuring and modeling carbon dioxide and water vapour exchange over a temperate broad-leaved forest during the 1995 summer drought. *Plant Cell Environ.,* **20,** 1108–1122.
——, and P. C. Harley, 1995: Scaling carbon dioxide and water vapour exchange from leaf to canopy in a deciduous forest: Model testing and application. *Plant Cell Environ.,* **18,** 1157–1173.
Ball, F. K., 1960: Control of inversion height by surface heating. *Quart. J. Roy. Meteor. Soc.,* **86,** 483–494.
Barradas, V. L., and H. G. Jones, 1996: Responses of CO_2 assimilation to changes in irradiance: Laboratory and field data and a model for beans. *J. Exp. Bot.,* **47,** 639–645.
Betts, A. K., 1973: Non-precipitating cumulus convection and its parameterization. *Quart. J. Roy. Meteor. Soc.,* **99,** 178–196.
——, 1984: Boundary layer thermodynamics of a high plains severe storm. *Mon. Wea. Rev.,* **112,** 2199–2211.
——, 1985: Mixing line analysis of clouds and cloudy boundary layers. *J. Atmos. Sci.,* **42,** 2751–2763.
——, 1992: Budget analyses of the FIFE atmospheric boundary layer. *J. Geophys. Res.,* **97,** 18 523–18 531.
——, and J. H. Ball, 1995: The FIFE surface diurnal cycle. *J. Geophys. Res.,* **100,** 25 679–25 693.
——, and A. G. Barr, 1996: First International Satellite Land Surface Climatology Field Experiment 1987 sonde budget revisited. *J. Geophys. Res.,* **101,** 23 285–23 288.
——, J. H. Ball, A. C. M. Beljaars, M. J. Miller, and P. A. Viterbo, 1996: The land surface–atmosphere interaction: A review based on observational and global modeling perspectives. *J. Geophys. Res.,* **101,** 7209–7225.
——, P. Viterbo, A. Beljaars, and B. van den Hurk, 1999: Use of field data to diagnose land-surface interaction. *Seminar on Designs of Models and Data Assimilation Systems,* Reading, United Kingdom, ECMWF, 347–364.
Brown, T. J., and B. L. Hall, 1999: The use of *t* values in climatological composite analyses. *J. Climate,* **12,** 2941–2944.
Burke, C. J., 1945: Transformation of polar continental air to polar maritime air. *J. Meteor.,* **2,** 94–112.
Businger, J. A., 1954: Some aspects of the influence of the earth's surface on the atmosphere. Chapter of Ph.D. thesis, Dept. of Natural Sciences and Art, University of Utrecht, Utrecht, Netherlands, 48–73.
Cardon, Z. G., J. A. Berry, and I. E. Woodrow, 1994: Dependence of the extent and direction of average stomatal response in *Zea mays* L. and *Phaseolus vulgaris* L. on the frequency of fluctuations in environmental stimuli. *Plant Physiol.,* **105,** 1007–1013.
Carlson, M. A., and R. B. Stull, 1986: Subsidence in the nocturnal boundary layer. *J. Climate Appl. Meteor.,* **25,** 1088–1099.
Carson, D. J., 1973: The development of a dry-inversion-capped convectively unstable boundary layer. *Quart. J. Roy. Meteor. Soc.,* **99,** 450–467.
Deardorff, J. W., 1972: Parameterization of the planetary boundary layer for use in general circulation models. *Mon. Wea. Rev.,* **100,** 93–106.
——, 1974: Three-dimensional numerical study of the height and mean structure of a heated planetary boundary layer. *Bound.-Layer Meteor.,* **7,** 81–106.
De Bruin, H. A. R., and A. A. M. Holtslag, 1982: A simple parameterization of the surface fluxes of sensible and latent heat during daytime compared with the Penman–Monteith concept. *J. Appl. Meteor.,* **21,** 1610–1621.
Driedonks, A. G. M., 1982: Models and observations of the growth of the atmospheric boundary layer. *Bound.-Layer Meteor.,* **23,** 283–306.
Ek, M., and L. Mahrt, 1994: Daytime evolution of relative humidity at the boundary layer top. *Mon. Wea. Rev.,* **122,** 2709–2720.
Fitzjarrald, D. R., 1982: New applications of a simple mixed layer model. *Bound.-Layer Meteor.,* **22,** 431–453.
——, 1997: Surface exchanges and air-mass modification. Preprints, *12th Symp. on Boundary Layers and Turbulence,* Vancouver, BC, Canada, Amer. Meteor. Soc., 587–588.
——, and G. G. Lala, 1989: Hudson Valley fog environments. *J. Appl. Meteor.,* **28,** 1303–1328.
——, and K. E. Moore, 1994: Growing season boundary layer climate and surface exchanges in a subarctic lichen woodland. *J. Geophys. Res.,* **99,** 1899–1917.
——, O. C. Acevedo, and K. E. Moore, 2001: Climatic consequences of leaf presence in the eastern United States. *J. Climate,* **14,** 598–614.
Foster, D., 1992: Land-use history (1730–1990) and vegetation dynamics in central New England, USA. *J. Ecol.,* **80,** 753–772.
Freedman, J. M., 2000: Surface–atmosphere exchange and boundary layer cumulus clouds. Ph.D. dissertation, Dept. of Earth and Atmospheric Sciences, University at Albany, State University of New York, 143 pp.
——, D. R. Fitzjarrald, K. E. Moore, and R. K. Sakai, 2001: Boundary layer clouds and vegetation–atmosphere feedbacks. *J. Climate,* **14,** 180–197.
Garratt, J. R., 1992: *The Atmospheric Boundary Layer.* Cambridge University Press, 316 pp.
Garstang, M., and D. R. Fitzjarrald, 1999: *Observations of Surface to Atmosphere Interactions in the Tropics.* Oxford University Press, 405 pp.
Harmon, J. R., 1987: Mean monthly North American anticyclone frequencies, 1950–79. *Mon. Wea. Rev.,* **115,** 2840–2848.
Holtslag, A. A. M., and A. P. van Ulden, 1983: A simple scheme for daytime estimates of the surface fluxes from routine weather data. *J. Climate Appl. Meteor.,* **22,** 517–529.
Huschke, R. E., 1959: *Glossary of Meteorology.* Amer. Meteor. Soc., 638 pp.
Liou, K.-N., 1992: *Radiation and Cloud Processes in the Atmosphere: Theory, Observation and Modeling.* Oxford University Press, 487 pp.
MacPherson, J. I., and A. K. Betts, 1997: Aircraft encounters with strong coherent vortices over the boreal forest. *J. Geophys. Res.,* **102,** 29 231–29 234.
Mahrt, L., 1976: Mixed layer moisture structure. *Mon. Wea. Rev.,* **104,** 1403–1418.
——, 1991: Boundary layer moisture regimes. *Quart. J. Roy. Meteor. Soc.,* **117,** 151–176.
Martin, C. L., D. Fitzjarrald, M. Garstang, A. P. Oliveira, S. Greco, and E. Browell, 1988: Structure and growth of the mixing layer over the Amazonian rain forest. *J. Geophys. Res.,* **93,** 1361–1375.
McNaughton, K. G., and T. W. Spriggs, 1985: A mixed-layer model for regional evaporation. *Bound.-Layer Meteor.,* **34,** 243–262.
Moore, K. E., D. R. Fitzjarrald, R. K. Sakai, M. L. Goulden, J. W. Munger, and S. C. Wofsy, 1996: Seasonal variations in radiative and turbulent exchange at a deciduous forest in central Massachusetts. *J. Appl. Meteor.,* **35,** 122–134.
——, ——, ——, and J.M. Freedman, 2001: Growing season water balance at a boreal jack pine forest. *Water Resour. Res.,* **36,** 483–493.
NWS, 1998: ASOS users guide. National Weather Service, National Oceanic and Atmospheric Administration, Silver Spring, MD, 61 pp.
Oke, T. R., 1987: *Boundary Layer Climates.* 2d. ed. Methuen, 435 pp.
Paluch, I. R., 1979: The entrainment mechanism in Colorado cumuli. *J. Atmos. Sci.,* **36,** 2467–2478.
Paulson, C. A., 1970. The mathematical representation of wind speed and temperatures in the unstable atmospheric surface layer. *J. Appl. Meteor.,* **9,** 857–861.
Pielke, R. A., Sr., 2000: Overlooked issues in the U.S. National Cli-

mate and IPCC assessments. Preprints, *11th Symp. on Global Change Studies,* Long Beach, CA, Amer. Meteor. Soc., 32–35.
Rabin, R. M., S. Stadler, P. J. Wetzel, D. J. Stensrud, and M. Gregory, 1990: Observed effects of landscape variability on convective clouds. *Bull. Amer. Meteor. Soc.,* **71,** 272–280.
Raupach, M. R., 1991: Vegetation–atmosphere interaction in homogeneous and heterogeneous terrain: Some implications of mixed-layer dynamics. *Vegetatio,* **91,** 105–120.
——, and J. J. Finnigan, 1988: Single-layer models of evaporation from plant canopies are incorrect but useful, whereas multilayer models are correct but useless: Discussion. *Aust. J. Plant Physiol.,* **15,** 705–716.
Rosenberg, N. J., B. L. Blad, and S. H. Verma, 1983: *Microclimate: The Biological Environment.* John Wiley and Sons, 495 pp.
Ruimy, A., B. Saugier, and G. Dedieu, 1994: Methodology for the estimation of terrestrial net primary production from remotely sensed data. *J. Geophys. Res.,* **99,** 5263–5283.
Sakai, R. K., D. R. Fitzjarrald, and K. E. Moore, 1997: Detecting leaf area and surface resistance during transition seasons. *Agric. For. Meteor.,* **84,** 273–284.
Sellers, P., F. G. Hall, G. Asrar, D. E. Strebel, and R. E. Murphy, 1992: An overview of the First ISLSCP Field Experiment. *J. Geophys. Res.,* **97,** 18 345–18 372.
——, and Coauthors, 1995: The Boreal Ecosystem–Atmosphere Study (BOREAS): An overview and early results from the 1994 field year. *Bull. Amer. Meteor. Soc.,* **76,** 1549–1577.
Stommel, H., 1947: Entrainment of air into a cumulus cloud. *J. Meteor.,* **4,** 91–94.
Stull, R. B., 1985: Models and measurements of the interaction between the mixed layer and fair-weather cumulus clouds. *The Meteorology of Acid Deposition,* P. J. Samson, Ed., Air Pollution Control Association, 140–147.
——, 1988: *An Introduction to Boundary Layer Meteorology.* Kluwer, 666 pp.
——, and E. Eloranta, 1985: A case study of the accuracy of routine, fair-weather cloud-base reports. *Natl. Wea. Dig.,* **10,** 19–24.
Su, X., 1998: Ozone temporal variations at Whiteface Mountain and processes responsible for these variations. Ph.D. dissertation, University at Albany, State University of New York, 168 pp.
Tennekes, H., 1973: A model for the dynamics of the inversion above a convective boundary layer. *J. Atmos. Sci.,* **30,** 558–567.
Wyngaard, J. C., and R. A. Brost, 1984: Top-down and bottom-up diffusion of a scalar in the convective boundary layer. *J. Atmos. Sci.,* **41,** 102–112.
Zhang, J., 1998: Influences of atmospheric transport and vertical mixing processes on ambient ozone levels in the northeastern United States. Ph.D. dissertation, University at Albany, State University of New York, 145 pp.